East European Journal of Physics. 4. 349-359 (2024)
DOI:10.26565/2312-4334-2024-4-40 ISSN 2312-4334

# UNVEILING THE POTENTIAL OF DOUBLE PEROVSKITE HALIDES $Rb_2CuSbH_6$ (H = Cl, Br, I) FOR FLEXIBLE ELECTRONICS: AN INTEGRATED STUDY OF STRUCTURAL, MECHANICAL, ELECTRICAL AND OPTICAL PROPERTIES

**Krishna Kumar Mishra[a]*, Sonia Chahar[a], Rajnish Sharma[b]**
[a]*Chitkara University Institute of Engineering and Technology, Chitkara University, Rajpura, Punjab-140401, India*
[b]*School of Engineering and Technology, Chitkara University, Solan, Himachal Pradesh-174103, India*
**Corresponding Author e-mail: krishna.mishra@chitkara.edu.in*
Received July 10, 2024; revised October 4, 2024; accepted October 29, 2024

The structural, mechanical, electrical and optical properties of double perovskite halides like $Rb_2CuSbH_6$ (where H = Cl, Br, and I) for flexible electronic devices are fascinating and complex. Extensive literature survey clearly establishes that there has been limited research on analyzing the potential uses of these materials for the highly sought-after sector of flexible electronic devices. In this paper, focused studies have been carried out on investigating the characteristics of these materials using QuantumATK NanoLab Software Tool. All double perovskite halides $Rb_2CuSbH_6$ (H = Cl, Br, I) show positive values for the elastic constants $C_{11}$, $C_{12}$, and $C_{44}$, and obey the stability trend $C_{11}>C_{12}>C_{44}$. Mechanical stability was established using Born-Huang criteria. Optimized values of Young's modulus, bulk modulus, shear modulus and Poisson ratios established that materials are stable and ductile in nature. While carrying out analysis of electronic properties, all three materials $Rb_2CuSbCl_6$, $Rb_2CuSbBr_6$, and $Rb_2CuSbI_6$ were found to be possessing indirect energy bandgap of 0.924 eV, 0.560 eV, and 0.157 eV, respectively. Moreover, the Complex Bandstructure (CB) naturality indicates that most evanescent wave may exist when layer separation is lowest in $Rb_2CuSbCl_6$ (6.0 Å), $Rb_2CuSbBr_6$ (6.33 Å), and highest in $Rb_2CuSbI_6$ (6.8 Å). Absorption bands for $Rb_2CuSbCl_6$, $Rb_2CuSbBr_6$ and $Rb_2CuSbI_6$ lie in the visible range with 344 nm to 574 nm, 348 nm to 688 nm and 369 nm to 608 nm respectively. The reflectivity (r) reported under this study is 0.105, 0.139 and 0.185 respectively for $Rb_2CuSbCl_6$, $Rb_2CuSbBr_6$ and $Rb_2CuSbI_6$. Overall, all the obtained results implicate toward need to explore the $Rb_2CuSbH_6$ materials in more depth for variety of electronic device applications.
**Keywords:** *Perovskite; QuantumATK; DFT; Optical Properties; Electronic structure; Mechanical properties*
**PACS:** 71.20.−b, 77.22.−d, 78.20.Ci

## 1. INTRODUCTION

Flexible electronic devices market is expected to grow at a Compound Annual Growth Rate (CAGR) of more than 15 % by year 2027 [1]. Advances in materials research, production, and design are continually changing flexible electronic device development. With its maturity, the technology is projected to alter healthcare and consumer electronics, enabling new smart, integrated, and highly flexible gadgets. Wearable technology, such as fitness trackers and smartwatches, has become increasingly popular, contributing significantly to the growth of the flexible electronics sector [2].

The materials used for flexible electronic devices are crucial for their functionality, durability, and flexibility [3,4]. A combination of variety of materials ultimately helps in creating a good flexible electronic device. Materials like Polyimide (PI), Polyethylene Terephthalate (PET), Polyethylene Naphthalate (PEN) are typically being used for flexible substrates. Indium Tin Oxide (ITO), Silver Nanowires, Graphene and Carbon nanotubes are used as conductive materials in the process of overall fabrication of the device. Many other materials like a-Si, indium gallium zinc oxide (IGZO), Barium Strontium Titanate (BST), polymethyl methacrylate etc. are used as conducting or dielectric materials [5]. Teflon and other specialized polymers have been used to protect devices from moisture and other environmental factors. Among all these materials, perovskites have been making their place owing to their ease of fabrication and display of high efficiency especially for solar cell devices [6-8]. The halide-based double perovskites have been explored in a number of different fields of application, including topological insulating materials [9], solar energy systems [10-14], and as superconductors [15]. Various studies have shown that Pb-halide perovskites can display an efficiency of more than 20% [16]. Efforts are being made to bring this conversion efficiency in the range of 45-50% [17].

Methylammonium lead iodide ($CH_3NH_3PbI_3$) has been investigated as a possible material for use in solar cell technology [18]. However, the material exhibited poor thermodynamic strength, showing a tendency to decompose into various phases, ultimately rendering it highly unstable [19, 20]. Perovskites have been successfully improved by using an ion exchange technique coupled with an ion exchange matrix to enhance their crystal structure in some cases [21, 22].

The double lead (Pb) halide perovskites have superior performance and technical superiority, as well as being highly efficient and cost-effective [23]. However, there remains a significant concern in the context of its instability and toxicity [24]. Pb-based perovskites are restricted from being used in photovoltaics because of this particular property. To overcome these difficulties, researchers are working on developing a perovskite-like material that does not contain lead but must have more manufacturing efficiency [25] and be capable of mixing cations [26], so as to achieve the capabilities of creating a perovskite. A good example of this is the use of organic halides in perovskites. It may be possible to reduce lead while maintaining bandgap by using DFT based computational method [27].

***Cite as:*** K.K. Mishra, S. Chahar, R. Sharma, East Eur. J. Phys. 4, 349 (2024), https://doi.org/10.26565/2312-4334-2024-4-40

In recent years, researchers have developed and characterized Cs-based double halides with exceptional light-absorbing properties [28, 29]. Despite this, Cs-based materials continue to be the subject of discussion and investigation because Cs is a scarce metal that presents a financial disadvantage in large-scale commercial production. The halides $Rb_2ScAgX_6$ and $Rb_2ScCuX_6$ (X = Cl, Br, I) have been studied extensively in the past one decade. A major reason for their potential use in thermoelectric and solar cell applications consists of their cost-effectiveness [30, 31]. The use of low-cost materials to customize Sc and Ag can have a significant impact on material science and the production of solar cells.

The $Rb_2CuSbH_6$ series offers an opportunity for the development of customized designs and improvements in functionality due to its adaptable composition that allows for the incorporation of different halogen substitutions such as Cl, Br, and I. It is likely that the inclusion of Cl, Br, and I substitutions in $Rb_2CuSbH_6$ will enhance application ranges and improve performance in several technical domains by taking into account small differences in its structure.

In this study, we investigate and understand the various characteristics of these halide perovskites. It describes their fundamental behaviours and identifies their possible applications for solar cells, optoelectronic devices and other flexible electronic devices.

## 2. COMPUTATIONS AND METHODOLOGY

In this study, the structural and electronic properties of double perovskite halides, $Rb_2CuSbH_6$ (H = Cl, Br, I), were systematically studied employing density functional theory (DFT) simulations. The computational work was carried out utilizing the QuantumATK software, employing its latest version (V-2023.09 SP1) [32]. The crystallographic data for $Rb_2CuSbH_6$, which crystallizes in the orthorhombic space group (Fm-3m), was sourced from the database of Materials Project. The DFT calculations employed the Generalized Gradient Approximation (GGA) method, utilizing the Perdew-Burke-Ernzerhof (PBE) functional for exchange-correlation interactions [33-34]. The linear combination of atomic orbitals (LCAO) approach was applied to represent the wave functions, with the numerical accuracy parameters adjusted to ensure precise results. Specifically, the density mesh cutoff was fixed at 105 Hartree, and the k-point grid was sampled using a (4×4×4) Monkhorst-Pack mesh. Fermi-Dirac smearing was used with a broadening of 1000 K and a convergence tolerance of 0.0001. The structural optimization and passivation processes were conducted in an iterative manner to ensure the stability and reliability of the crystal structures. For the pseudopotentials [35], PseudoDojo projector-augmented wave (PAW) potentials were utilized, assigning suitable potentials for each constituent element: Rubidium (Z=9), Copper (Z=19), Antimony (Z=23), Chlorine (Z=7), Bromine (Z=7), and Iodine (Z=7). To accurately solve the electronic structure and determine the energy levels, the diagonalization solver was employed to address the eigenvalue problems, ensuring precise electronic property calculations.

## 3. RESULTS AND DISCUSSION

### A. STRUCTURAL AND MECHANICAL PROPERTIES

The computational analysis in this study was conducted using the QuantumATK software, version V-2023.09 SP1 [32]. To model the exchange-correlation interactions, the Generalized Gradient Approximation (GGA) was applied, specifically utilizing the Perdew-Burke-Ernzerhof (PBE) functional. The Linear Combination of Atomic Orbitals (LCAO) method was employed for calculating electronic properties. For enhanced precision, a density mesh cutoff of 105 Hartree was used, and the k-point grid was sampled with a (4×4×4) Monkhorst-Pack mesh. Fermi-Dirac statistics were applied with a broadening of 1000 K and a convergence tolerance of 0.0001. Pseudopotentials from the PseudoDojo library were employed for the respective elements in the crystal structure, including Rubidium (Z=9), Copper (Z=19), Antimony (Z=23), Chlorine (Z=7), Bromine (Z=7), and Iodine (Z=7). The structural bonding and atomic arrangements of the double perovskite halide $Rb_2CuSbH_6$ (where H = Cl, Br, I) are illustrated in Figures 1(a) and 1(b) as part of Figure 1, providing a detailed depiction of the material's crystal structure.

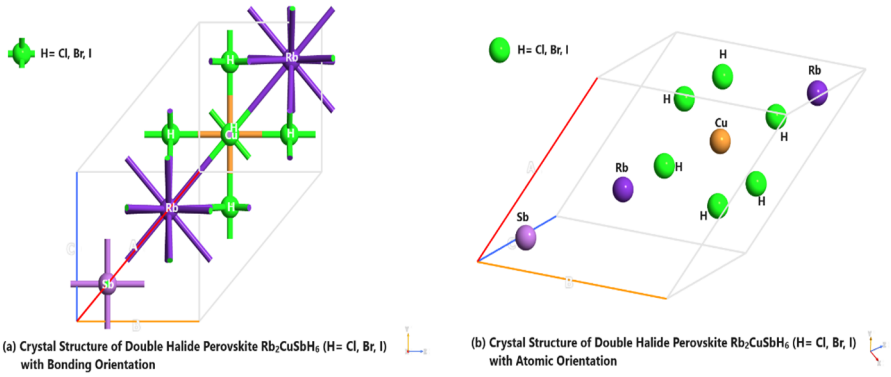


**Figure 1.** Crystal Structure of double halide $Rb_2CuSbH_6$ (H= Cl, Br, I)

There are twelve equivalent $RbH_{12}$ cuboctahedra, six equivalent $RbH_{12}$ cuboctahedra, four equivalent $CuH_6$ octahedra, and four equivalent $SbH_6$ octahedra formed when $Rb^{1+}$ bonds to 12 $H^{1-}$ atoms. The Rb–H bond lengths for $Rb_2CuSbCl_6$, $Rb_2CuSbBr_6$ and $Rb_2CuSbI_6$ are respectively 3.68 Å, 3.88 Å, and 4.17 Å. For $Rb_2CuSbCl_6$, $Rb_2CuSbBr_6$

and $Rb_2CuSbI_6$, the lengths of the Cu–H bonds for each of these compounds are 2.52 Å, 2.65 Å, and 2.85 Å respectively. All Sb–H bond lengths are 2.68 Å, 3.86 Å and 4.17 Å for $Rb_2CuSbCl_6$, $Rb_2CuSbBr_6$ and $Rb_2CuSbI_6$ respectively. $Rb_2CuSbCl_6$, $Rb_2CuSbBr_6$ and $Rb_2CuSbI_6$ have Cl-Cl, Br-Br and I-I bond lengths of 3.57 Å, 3.75 Å, and 4.03 Å respectively. Four $Rb^{1+}$ atoms, one $Cu^{1+}$ atom, and one $Sb^{3+}$ atoms are bonded to $H^{1-}$ in a distorted linear geometry.

The equilibrium lattice contacts ($a_0$) and elastic constants ($C_{ij}$) for double perovskite halides $Rb_2CuSbH_6$ (H = Cl, Br, I) are shown in Table 1. According to results, the lattice constant, unit cell volume and density increase from $Rb_2CuSbCl_6$ to $Rb_2CuSbBr_6$ to $Rb_2CuSbI_6$. The reported values of lattice constant are 10.41 Å, 10.97 Å and 11.79 Å for $Rb_2CuSbCl_6$, $Rb_2CuSbBr_6$ and $Rb_2CuSbI_6$ respectively. Our results are consistent with other studies [36, 37] as mentioned in table 1. It is evident that this increasing variation in lattice constant ($a_0$), volume and density of unit cell are consistent with the change as the ion radius increases. There is a benefit to using alkali atoms, which are lighter, as they can minimize the density of the material, which is used as a perovskite, which can reduce the weight of a device. The reliability of our geometry optimization was confirmed through a thorough comparison with previous published results [36, 37].

**Table 1.** Computed equilibrium lattice ($a_0$) and elastic ($C_{ij}$) constants for $Rb_2CuSbH_6$ (H= Cl, Br, I)

| Materials | $a_0$(Å) | Unit Cell Volume (Å$^3$) | Density (g/cm$^3$) | Space Group | $C_{11}$ (GPa) | $C_{12}$ (GPa) | $C_{44}$ (GPa) |
|---|---|---|---|---|---|---|---|
| **$Rb_2CuSbCl_6$** | **Present Study** | 10.41 | 282.4 | 3.346 | 44.69 | 23.95 | 12.20 |
| | **Other Study (Exp. & Theo.)** | 10.23 [36]<br>10.19 [37] | - | 3.57 [37] | 52.26 [36] | 27.90 [36] | 12.34 [36] |
| **$Rb_2CuSbBr_6$** | **Present Study** | 10.97 | 330.5 | 4.199 | 33.98 | 28.26 | 9.73 |
| | **Other Study (Exp. & Theo.)** | 11.00 [36] | - | - | - | - | - |
| **$Rb_2CuSbI_6$** | **Present Study** | 11.79 | 409.6 | 4.531 | 8.98 | 30.33 | 7.23 |
| | **Other Study (Exp. & Theo.)** | 11.81 [36] | - | - | - | - | - |

The elastic properties of the cubic crystal structures are determined by three independent elastic constants shown in Table 01. All double perovskite halides $Rb_2CuSbH_6$ (H = Cl, Br, I) show positive values for the elastic constants $C_{11}$, $C_{12}$, and $C_{44}$, and obey the stability trend $C_{11}>C_{12}>C_{44}$. Born-Huang stability criterion was used to assess mechanical stability of these materials [38, 39]: (a) $C_{11}>0$ (b) $C_{11}-C_{12}>0$ (c) $C_{11}+2C_{12}>0$ (d) $C_{44}>0$. Mechanical stability criteria are met by these materials, making them stable. The computed positive value of Cauchy's pressures $C_{12}-C_{44}$ concludes that all double perovskite halides (DPHs) $Rb_2CuSbH_6$ (H = Cl, Br, I) are ionic in nature. Below table 2 showcased the material properties from the elastic constants (GPa) for $Rb_2CuSbH_6$ (H= Cl, Br, I).

**Table 2.** Computed material properties from the elastic constants (GPa) for $Rb_2CuSbH_6$ (H= Cl, Br, I)

| Materials | | Bulk modulus (GPa) | Shear modulus (GPa) | Young's modulus (GPa) | Poisson ratios |
|---|---|---|---|---|---|
| **$Rb_2CuSbCl_6$** | **Present Study** | 30.86 | 11.39 | 27.97 | 0.34 |
| | **Other Study (Exp. & Theo.)** | 37.38 [36]<br>36.02 [37] | 12.28 [37] | | 0.347 [37] |
| **$Rb_2CuSbBr_6$** | **Present Study** | 30.17 | 4.96 | 8.32 | 0.45 |
| | **Other Study (Exp. & Theo.)** | 27.60 [36] | | | |
| **$Rb_2CuSbI_6$** | **Present Study** | 23.21 | 21.99 | 37.82 | 0.77 |
| | **Other Study (Exp. & Theo.)** | 21.28 [36] | | | |

## B. ELECTRONIC PROPERTIES

Solar cells and light-emitting diodes are both efficient due to the influence of band structure on carrier transitions and movement, optical absorption coefficients, as well as electrical conductivity. In order to design optoelectronic devices, it's important to understand the band structure thoroughly. Energy Bandstructure of DPHs $Rb_2CuSbH_6$ (H= Cl, Br, I) are depicted in Figure 2(a)-(c) for $Rb_2CuSbCl_6$, $Rb_2CuSbBr_6$ and $Rb_2CuSbI_6$ respectively.

Interestingly, all three double perovskite halides have indirect bandgaps. For all compounds, the valence and conduction bands are at X and L symmetry. The indirect band gaps of $Rb_2CuSbCl_6$, $Rb_2CuSbBr_6$, and $Rb_2CuSbI_6$ are 0.924 eV, 0.560 eV, and 0.157 eV, respectively. Effective curvature represents the effective mass (m*) of carriers in these bands. Effective charge carriers in the valence band with a flat or dense state have a high effective mass, but with a high curvature in the conduction band states, electrons have a smaller effective mass, which makes optoelectronic devices more efficient. All the three double perovskite halides $Rb_2CuSbH_6$ (H= Cl, Br, I) are having a narrow band-gap semiconducting property. The study results revealed that the double perovskite halides $Rb_2CuSbH_6$ (H = Cl, Br, I) can be combined with wide-gap materials to improve the record of conversion efficiency in tandem solar cells.

The Complex Bandstructure (CB) consists of propagating and decaying modes, characterized by $k_c$. We analyzed a 2D CB to assess the materials for optical device and other photovoltaic applications [40-42]. Figure 3 illustrates the Complex Bandstructure of the double halides (a) $Rb_2CuSbCl_6$, (b) $Rb_2CuSbBr_6$, and (c) $Rb_2CuSbI_6$.

The variable $k_c$ can be complex on surfaces in the c-direction. Real *kc* values represent traditional Bloch states (right diagram), while complex $k_c$ values indicate surface states. The left graph shows the imaginary part, representing decay magnitude, with color codes indicating the real component of $k_c$.

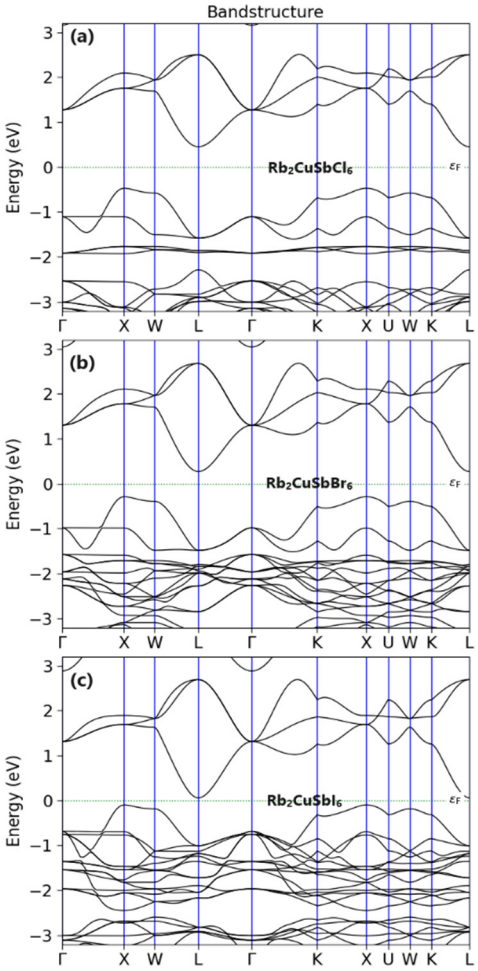


**Figure 2.** Energy Band structure of double perovskite halides $Rb_2CuSbH_6$ (H= Cl, Br, I) (a) $Rb_2CuSbCl_6$ (Eg=0.924 eV); (b)$Rb_2CuSbBr_6$ (Eg=0.560 eV); (c) $Rb_2CuSbI_6$ (Eg= 0.157 eV)

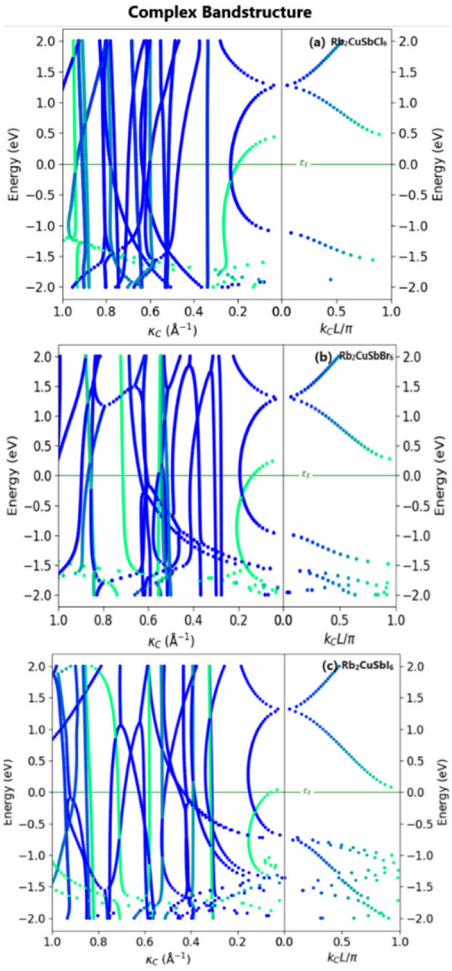


**Figure 3.** Complex Bandstructure of double perovskite halides $Rb_2CuSbH_6$ (a) $Rb_2CuSbCl_6$; (b) $Rb_2CuSbBr_6$; (c) $Rb_2CuSbI_6$

The analysis of the Complex Bandstructure (CB) reveals that only a few decaying modes are present in the right section, indicating the existence of evanescent waves on the material's surface. Our study indicates that double perovskite halides $Rb_2CuSbH_6$ materials are extremely appropriate for optoelectronic device fabrications. The nature of the CB shows that evanescent waves are favored due to the minimal layer separation, which is lowest in $Rb_2CuSbCl_6$ (6.01 Å), followed by $Rb_2CuSbBr_6$ (6.33 Å), and highest in $Rb_2CuSbI_6$ (6.8 Å). Thus, double perovskite halides $Rb_2CuSbH_6$ (H = Cl, Br, I) are promising candidates for optoelectronic and thermoelectric devices.

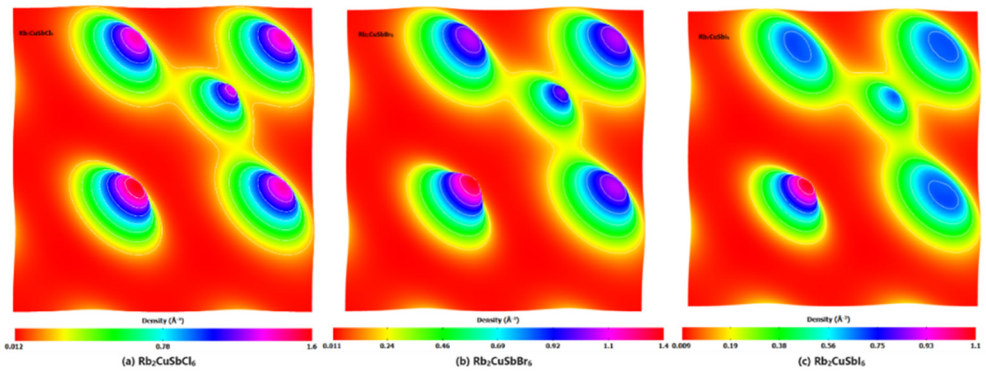


**Figure 4.** Electron density of double halide $Rb_2CuSbH_6$ (a) $Rb_2CuSbCl_6$; (b) $Rb_2CuSbBr_6$; (c) $Rb_2CuSbI_6$

We further investigated the electron density of these compounds to augment the results on the energy band and complex band. The electron density of double halide $Rb_2CuSbCl_6$, $Rb_2CuSbBr_6$ and $Rb_2CuSbI_6$ respectively are plotted in Figure 4 (a)-(c). As shown in Figure 4(a)-(c), electron density plots provide an insightful depiction of bonding nature. $Rb_2CuSbCl_6$ exhibits covalent bonding between Cu, Cl, and Sb atoms, while Rb atoms exhibit ionic characteristics. Simultaneously, the same covalent character is observed in $Rb_2CuSbBr_6$ and $Rb_2CuSbI_6$.

Further, $Rb_2CuSbCl_6$ has highest electron density 1.6 $Å^{-3}$ and $Rb_2CuSbI_6$ has the lowest 1.1 $Å^{-3}$. The major contribution is due to halides radii. The electron density reported decreasing with increase of atomic radii of the halides. Based on Figure 5(a)-(c) and Figure 6(a)-(c), an analysis of each element's contributions to valence and conduction bands can be done in more detail. The band structure near Fermi level is used to determine VBM and CBM contributions. Alkali metal Rb plays a small role in VBM and CBM; its primary role is to stabilize the perovskite structure by serving as a charge donor.

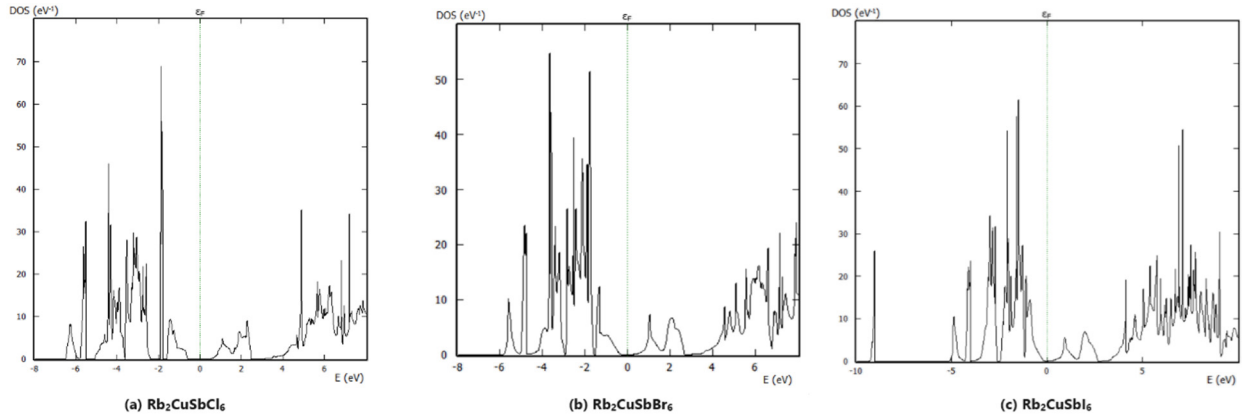


**Figure 5.** Density of States of double halide $Rb_2CuSbH_6$ (a) $Rb_2CuSbCl_6$; (b) $Rb_2CuSbBr_6$; (c) $Rb_2CuSbI_6$

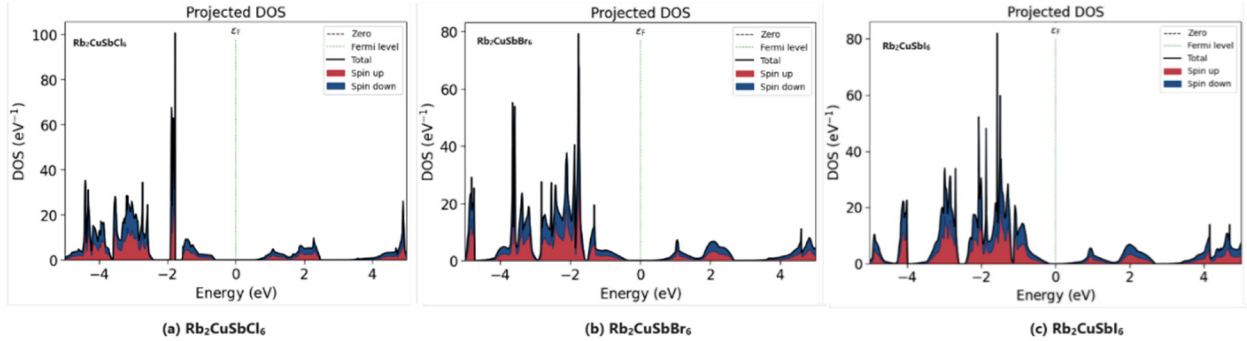


**Figure 6.** Projected Density of States of double halide $Rb_2CuSbH_6$ (a) $Rb_2CuSbCl_6$; (b) $Rb_2CuSbBr_6$; (c) $Rb_2CuSbI_6$

A main contribution to the VBM is the H-p orbital, and a major contribution to the CBM is the Sb-p orbital, with partial contributions from Cu-s and H-p orbitals. VBM and CBM electronic transition is primarily dominated by p and d orbitals which is evident from Figure 5(a)-(c) and 6(a)-(c).

## C. OPTICAL PROPERTIES

The optical properties of optoelectronic solid materials are incredibly important, including absorption, refractive index, reflectivity, and extinction loss [43]. To understand interaction between light and matter, we evaluated the optical characteristics of these double perovskite halides $Rb_2CuSbH_6$ (H= Cl, Br, I). The optical properties in this study are presented in two sets: (i) Real and (ii) Complex Optical Properties and are tabulated in Table 3 along with other studies done so far [36, 37].

Figure 7 (a)-(d) show the comparative study of Real Optical properties (a) absorption coefficients ($\alpha_a$), (b) Refractive Index ($n$), (c) Extinction Coefficient ($k$) and (d) Reflectivity ($r$), of double halide $Rb_2CuSbH_6$ (H=Cl, Br, I) respectively. Figure 7(a) indicates the absorption bands of double halide $Rb_2CuSbH_6$ (H=Cl, Br, I) and reported a highest pick at 3.36 eV (697589 $cm^{-1}$) 2.4 eV (648741 $cm^{-1}$) and 2.8 eV (597548 $cm^{-1}$) for $Rb_2CuSbCl_6$, $Rb_2CuSbBr_6$ and $Rb_2CuSbI_6$ respectively. Further, we have also calculated plotted the absorption coefficients with respect to wavelength (inset plot with x-axes as wavelength) and found that all the absorption bands lie in the visible range with 344 nm to 574 nm, 348 nm to 688 nm and 369 nm to 608 nm for $Rb_2CuSbCl_6$, $Rb_2CuSbBr_6$ and $Rb_2CuSbI_6$ respectively and align closely with earlier published results [37]. This justifies that these double halide $Rb_2CuSbH_6$ (H=Cl, Br, I) possess utmost important property for its solar applications.

**Table 3.** Computed optical properties for double perovskite halides $Rb_2CuSbH_6$ (H= Cl, Br, I)

| *Computed Optical Properties* | | *Materials* | | | | | | |
|---|---|---|---|---|---|---|---|---|
| | | | *$Rb_2CuSbCl_6$* | | *$Rb_2CuSbBr_6$* | | *$Rb_2CuSbI_6$* | |
| | | *Units* | *Present Study* | *Other Study (Exp. & Theo.)* | *Present Study* | *Other Study (Exp. & Theo.)* | *Present Study* | *Other Study (Exp. & Theo.)* |
| *Real Optical Properties* | *Absorption Coefficients ($\alpha_a$)* | *$cm^{-1}$* | 697589 (3.36 eV) | $6.12\times10^4$ [37] | 648741 (2.4 eV) | | 597548 (2.8 eV) | |
| | *Refractive Index (n)* | - | 1.96 | | 2.19 | | 2.51 | |
| | *Extinction Coefficient (k)* | - | $8.0\times10^{-5}$ | | $5.3\times10^{-5}$ | | $6.20\times10^{-5}$ | |
| | *Reflectivity (r)* | - | 0.105 | | 0.139 | | 0.185 | |
| *Complex Optical Properties* | *Dielectric constant (ε)* | - | 3.85 | 4.23 [37] | 4.79 | | 6.30 | |
| | *Susceptibility (χ)* | - | 2.85 | | 3.79 | | 5.30 | |
| | *Polarizability (α)* | *$C.m^2V^{-1}$* | $0.71\times10^{-38}$ | | $1.11\times10^{-38}$ | | $1.9\times10^{-38}$ | |
| | *Optical Conductivity (σ)* | *$A.V^{-1}cm^{-1}$* | $3.53\times10^3$ | $1.9\times10^4$ [36] | $4.23\times10^3$ | $7.8\times10^4$ [36] | $3.6\times10^3$ | $8.2\times10^4$ [36] |

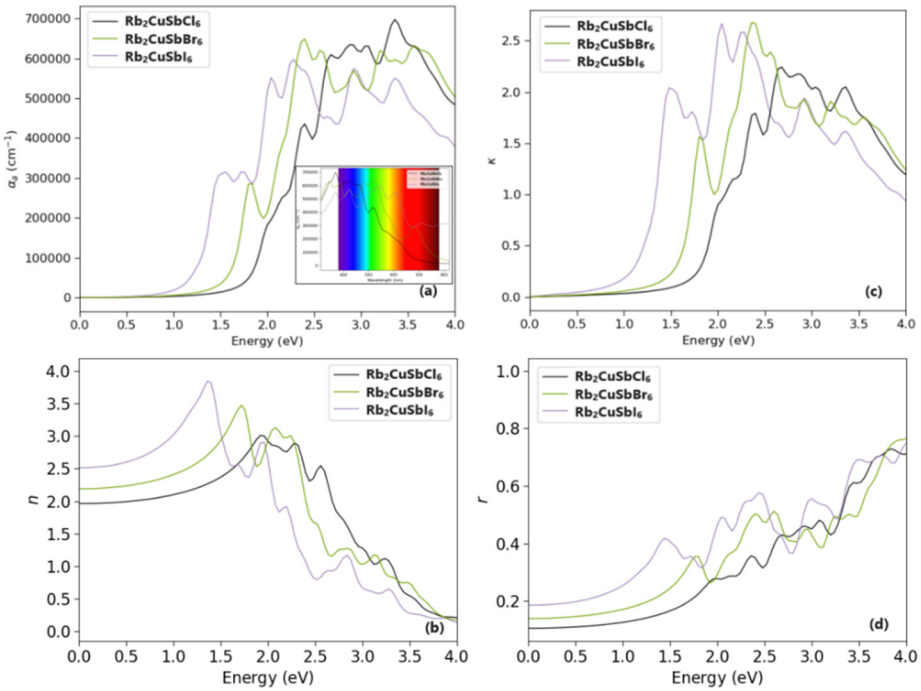


**Figure 7.** Real Optical properties (Absorption, Refractive Index, Extinction Coefficients and Reflectivity) of double halide $Rb_2CuSbH_6$ (H=Cl, Br, I) (a) Absorption, (b) Refractive Index, (c) Extinction Coefficients and (d) Reflectivity

The refractive index is a key factor in optics, as it provides information about how light interacts with a material. It changes depending on the speed at which light travels through different media [44]. Figure 7(b) illustrates the correlation between refractive index and energy, offering valuable insights into the optical behavior of the material across different energy ranges. The Computed value of refractive index (at 0 eV) from the plot are 1.96, 2.19 and 2.51 respectively for $Rb_2CuSbCl_6$, $Rb_2CuSbBr_6$ and $Rb_2CuSbI_6$. Whereas the observed peak values of refractive index are 3.01 at 1.92eV for $Rb_2CuSbCl_6$; 3.47 at 1.725 eV for $Rb_2CuSbBr_6$ and 3.89 at 1.36 eV for $Rb_2CuSbI_6$ respectively. For the high energy spectrum, specially above the 2.08 eV, 2.4 eV and 2.72 eV respectively for $Rb_2CuSbCl_6$, $Rb_2CuSbBr_6$ and $Rb_2CuSbI_6$, the value of refractive index (n) values decreases below 2.0 which makes these materials best fit for solar technology (refractive index (n) benchmark for solar cell technology, n = 1.0-2.0).

The absorption capability of a material at a specific frequency can be evaluated through its extinction coefficient, which defines how electromagnetic waves propagate within the material [45]. As shown in Figure 7(c), the extinction coefficient (*k*) follows a similar trend to the Kramer-Kronig relationship with energy. The observed values of extinction coefficient are $8.0\times10^{-5}$, $5.3\times10^{-5}$ and $6.20\times10^{-5}$ for $Rb_2CuSbCl_6$, $Rb_2CuSbBr_6$ and $Rb_2CuSbI_6$. The minimal variation in *k* suggests these compounds are excellent candidates for solar and optoelectronic devices, particularly in the higher energy regions above 2.08 eV, 2.4 eV, and 2.72 eV, respectively, for each material (in the order of $Rb_2CuSbCl_6$, $Rb_2CuSbBr_6$ and $Rb_2CuSbI_6$).

Figure 7(d) illustrates the reflectivity (*r*) of the materials, which provides essential insights into how they interact with light at the surface. The reported values of reflectivity (*r*) under this study for $Rb_2CuSbCl_6$, $Rb_2CuSbBr_6$ and

$Rb_2CuSbI_6$ are 0.105, 0.139 and 0.185 respectively. The reflectivity (*r*) possesses the similar trend as refractive index has i.e. the value of *r* increases with heavier atom substitution.

Additionally, the complex optical properties of these double perovskite halides $Rb_2CuSbH_6$ (H= Cl, Br, I) were analyzed to better understand their optical properties. Both the real (Re[ε]) and imaginary (Im[ε]) parts of the dielectric function are closely linked to the energy-dependent electronic transitions within the band structure. The complex dielectric function is defined as ε=Re[ε]+Im[ε] [46]. The spectra in Figure 8(a)-(c) are compared for the double halide $Rb_2CuSbH_6$ (H=Cl, Br, I) in energy ranges of 0-4 eV. The value of real dielectric function Re[ε] for $Rb_2CuSbCl_6$, $Rb_2CuSbBr_6$ and $Rb_2CuSbI_6$ are 3.85, 4.79 and 6.30 respectively. The values of basic real dielectric function Re[ε] increases with increase of the atomic radii moving from Cl→I. Also, the values of imaginary dielectric function Im[ε] is in parity with refractive index (n). The results of this study and characteristics are in good agreement with other studies [37] as well.

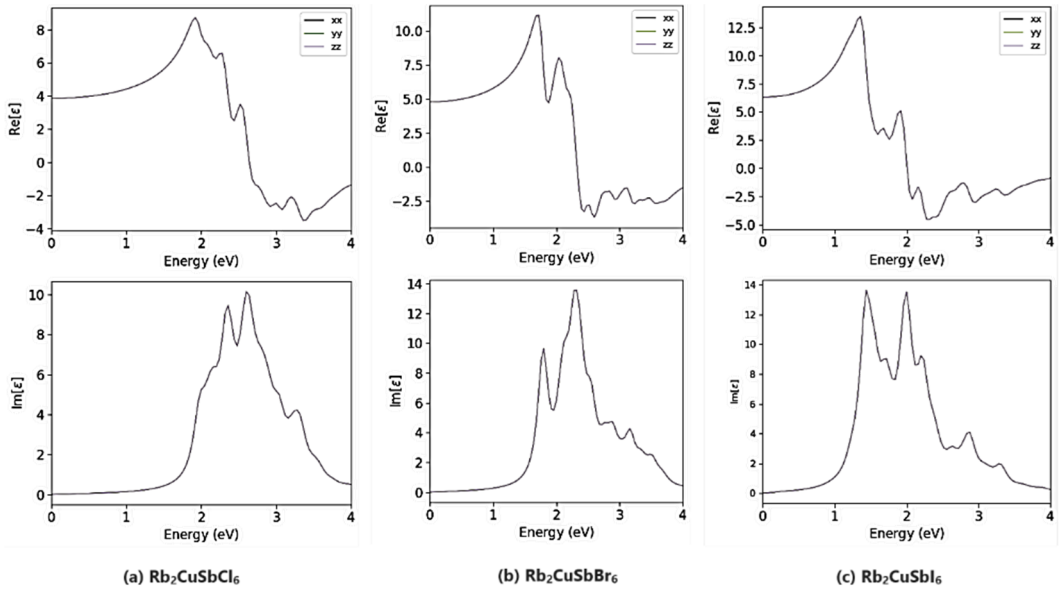


**Figure 8.** Dielectric Constant of double halide $Rb_2CuSbH_6$ (a) $Rb_2CuSbCl_6$; (b) $Rb_2CuSbBr_6$; (c) $Rb_2CuSbI_6$

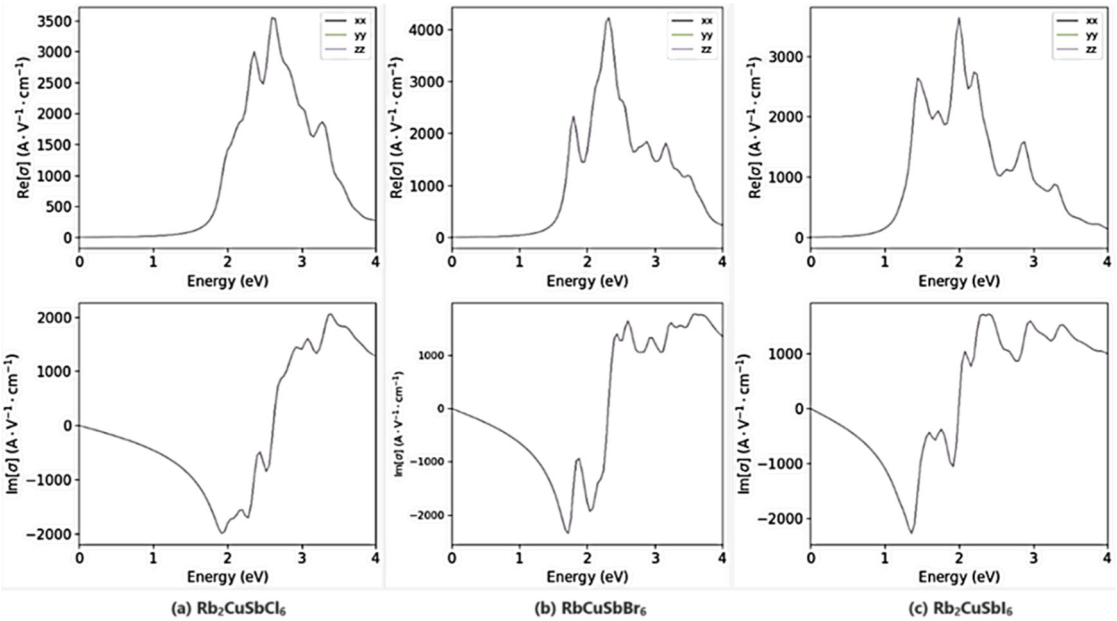


**Figure 9.** Optical Conductivity of double halide $Rb_2CuSbH_6$ (a) $Rb_2CuSbCl_6$; (b) $Rb_2CuSbBr_6$; (c) $Rb_2CuSbI_6$

Material optical conductivity is related to the magnitude of induced electric fields. The optical conductivity has been found to be $3.53\times10^3$ $AV^{-1}cm^{-1}$, $4.23\times10^3$ $AV^{-1}cm^{-1}$ and $3.6\times10^3$ $AV^{-1}cm^{-1}$ respectively for $Rb_2CuSbCl_6$, $Rb_2CuSbBr_6$ and $Rb_2CuSbI_6$ as shown in Figure 9(a)-(c). The results are in excellent agreement with other results [36] and suggest that these materials are excellent choice of material for optoelectronic devices. The polarizability of double halide $Rb_2CuSbH_6$ (H=Cl, Br, I) is also computed and represented in Figure 10(a)-(c). The polarizability is found to increasing with heavy halogen moving from $Rb_2CuSbCl_6$ → $Rb_2CuSbBr_6$ → $Rb_2CuSbI_6$ with the values $0.71\times10^{-38}$ $C\cdot m^2V^{-1}$, $1.11\times10^{-38}$ $C\cdot m^2V^{-1}$

and $1.9\times10^{-38}$ $C\cdot m^2V^{-1}$ respectively. We have also calculated the Susceptibility of these double halide $Rb_2CuSbH_6$ (H=Cl, Br, I) as shown in Figure 11(a)-(c) and found an increasing trend from $Rb_2CuSbCl_6$ → $Rb_2CuSbBr_6$ → $Rb_2CuSbI_6$ with the values 2.85, 3.79 and 5.30 respectively which makes these material appealing for storage devices.

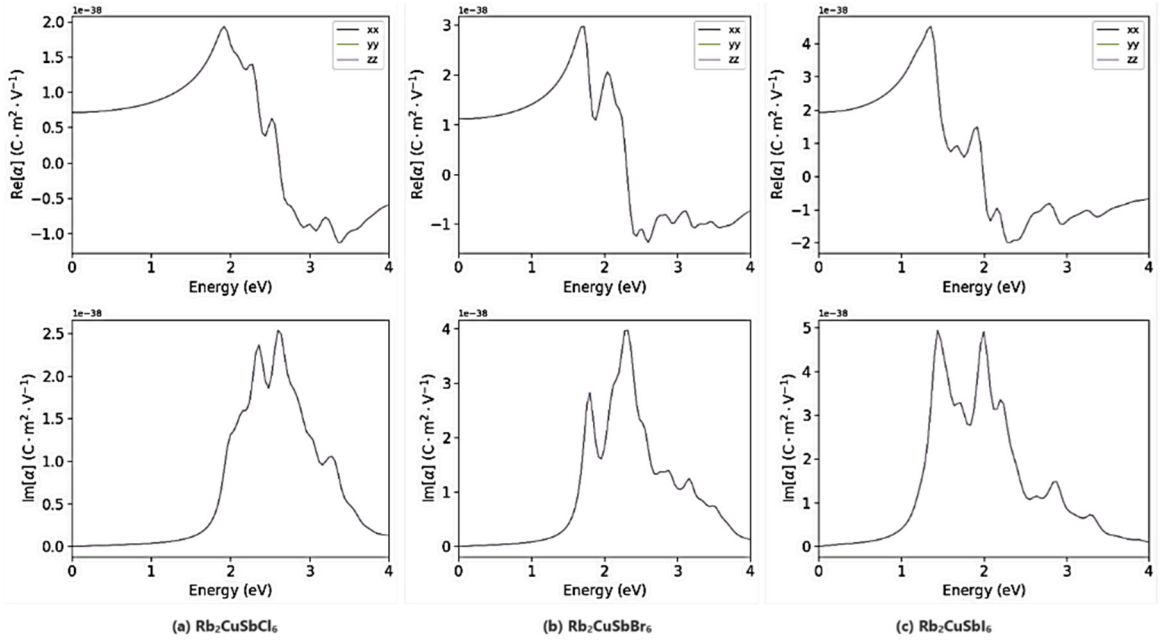


**Figure 10.** Polarizability of double halide $Rb_2CuSbH_6$ (a) $Rb_2CuSbCl_6$; (b) $Rb_2CuSbBr_6$; (c) $Rb_2CuSbI_6$

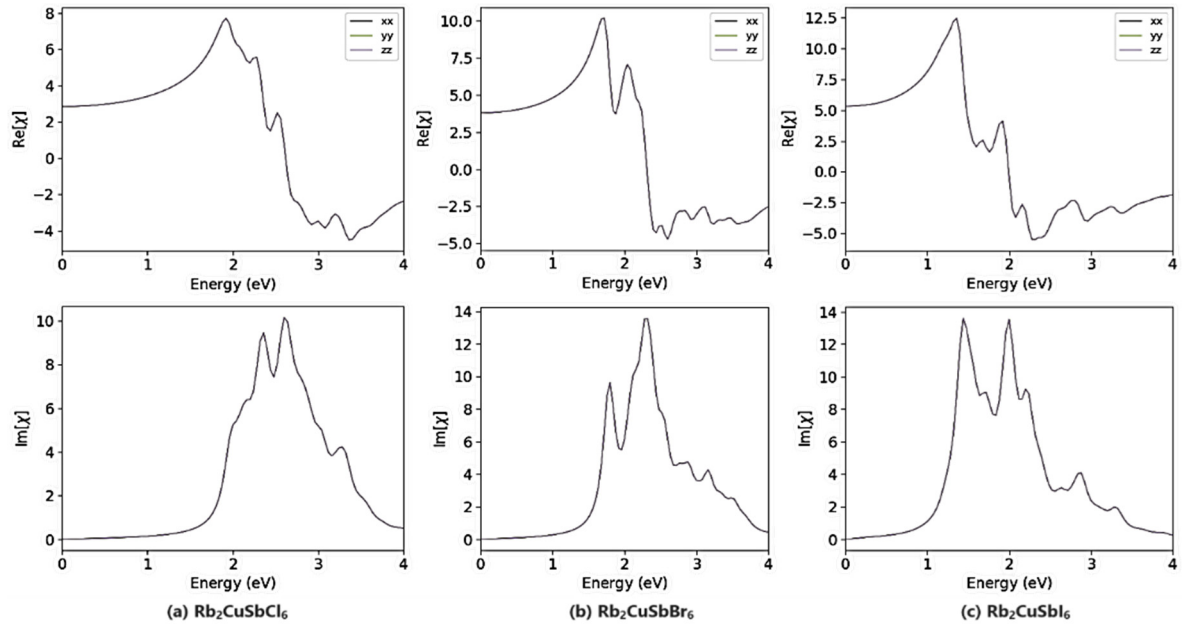


**Figure 11.** Susceptibility of double halide $Rb_2CuSbH_6$ (a) $Rb_2CuSbCl_6$; (b) $Rb_2CuSbBr_6$; (c) $Rb_2CuSbI_6$

## 4. CONCLUSIONS

The research on $Rb_2CuSbH_6$ (where H = Cl, Br, I) was carried out using DFT with the QuantumATK software, programmed in Python. The structural characteristics of these double perovskite halides were determined using DFT calculations based on the GGA and PBE functionals, employing the LCAO method. The key findings from this study are as follows:

1. The lattice constant ($a_0$), volume, and density of the unit cell for $Rb_2CuSbH_6$ increase progressively from $Rb_2CuSbCl_6$ to $Rb_2CuSbBr_6$ to $Rb_2CuSbI_6$. This trend is consistent with the increasing ionic radius of the halide ions. Additionally, incorporating alkali atoms can further reduce the material's overall density.

2. All double perovskite halides $Rb_2CuSbH_6$ (H = Cl, Br, I) show positive values for the elastic constants $C_{11}$, $C_{12}$, and $C_{44}$, and obey the stability trend $C_{11}>C_{12}>C_{44}$. The Born-Huang stability criterion was used to assess mechanical stability of these materials.

3. All three double perovskite halides have indirect bandgaps and have a narrow band-gap semiconducting property. Pairing the double perovskite halides $Rb_2CuSbH_6$ (H = Cl, Br, I) with high-bandgap compounds could improve the energy conversion efficiency of tandem solar cells.

4. Double perovskite halides $Rb_2CuSbH_6$ (H= Cl, Br, I) exhibit significant potential for applications in optoelectronic and thermoelectronic devices. The characteristics of the Complex Bandstructure (CB) indicate a conducive environment for the formation of evanescent waves on the surface of these materials.

5. We evaluated the optical properties of double perovskite halides $Rb_2CuSbH_6$ (H=Cl, Br, I) and found that the absorption bands of these materials lie in the visible range with 344 nm to 574 nm, 348 nm to 688 nm and 369 nm to 608 nm respectively.

6. The refractive index of $Rb_2CuSbCl_6$, $Rb_2CuSbBr_6$, and $Rb_2CuSbI_6$ drops below 2.0 in the high-energy spectrum. Their extinction coefficient, which helps determine absorption at specific frequencies, follows a similar energy-dependent trend as the Kramers-Kronig relations. Reflectivity increases with heavier atom substitution, with values of 0.105, 0.139, and 0.185 for $Rb_2CuSbCl_6$, $Rb_2CuSbBr_6$, and $Rb_2CuSbI_6$, respectively.

7. The optical properties of $Rb_2CuSbH_6$ (H = Cl, Br, I) were analyzed, showing that the real dielectric function (Re[ε]) values are 3.85, 4.79, and 6.30 for $Rb_2CuSbCl_6$, $Rb_2CuSbBr_6$, and $Rb_2CuSbI_6$, respectively. These are linked to frequency-dependent electronic transitions within the material.

8. We have calculated the polarizability and susceptibility of double halide $Rb_2CuSbH_6$ (H=Cl, Br, I) and found an increasing trend from $Rb_2CuSbCl_6$ $Rb_2CuSbBr_6$ $Rb_2CuSbI_6$ respectively.

The findings from this research are anticipated to provide valuable insights into potential uses for photovoltaic systems, electronic devices with optical components, and flexible electronics. This could pave the way for more cost-effective and efficient methods of utilizing solar power. Additionally, it may contribute to the creation of more adaptable and wearable technologies. The outcomes could also support the innovation of novel materials tailored for solar energy systems and various electronic applications.

## ORCID

**Krishna Kumar Mishra,** https://orcid.org/0000-0001-6888-7654; **Sonia Chahar,** https://orcid.org/0000-0001-5250-5228
**Rajnish Sharma,** https://orcid.org/0000-0001-8644-016X

## REFERENCES

[1] Flexible Electronics Global Market Report (2023). https://www.globenewswire.com/news-release/2023/03/14/2626974/0/en/Flexible-Electronics-Global-Market-Report-2023.html
[2] M.A. Amin, *et al*., "Study of double perovskites $X_2InSbO_6$ (X= Sr, Ba) for renewable energy; alternative of organic-inorganic perovskites," Journal of Materials Research and Technology, **18**, 4403-4412 (2022). https://doi.org/10.1016/j.jmrt.2022.04.114
[3] Q. Mahmood, M. Younas, M.G.B. Ashiq, S.M. Ramay, A. Mahmood, and H.M. Ghaithan, "First principle study of lead-free double perovskites halides $Rb_2Pd(Cl/Br)_6$ for solar cells and renewable energy devices: a quantum DFT," International Journal of Energy Research, **45**(10), 14995-15004 (2021). https://doi.org/10.1002/er.6778
[4] C. Zhang, *et al*., "Design of a novel and highly stable lead-free $Cs_2NaBiI_6$ double perovskite for photovoltaic application," Sustainable energy & fuels, **2**(11), 2419-2428 (2018). https://doi.org/10.1039/C8SE00154E
[5] A. Moskvin, L. Makhnev, N. Nomerovannaya, Loshkareva, and A. Balbashov, "Interplay of p-d and d-d charge transfer transitions in rare-earth perovskite manganites," Physical Review B, **82**(3), 035106 (2010). https://doi.org/10.1103/PhysRevB.82.035106
[6] C. Weeks, and M. Franz, "Topological insulators on the Lieb and perovskite lattices," Physical Review B, 82(8), 085310 (2010). https://doi.org/10.1103/PhysRevB.82.085310
[7] T. Yamada, *et al*., "Self-assembled perovskite-fluorite oblique nanostructures for adaptive (tunable) electronics," Advanced Materials, **21**(13), 1363-1367 (2009). https://doi.org/10.1002/adma.200800253
[8] J. Lettieri, M. Zurbuchen, Y. Jia, D. Schlom, S. Streiffer, and M. Hawley, "Epitaxial growth of non-c-oriented $SrBi_2Nb_2O_9$ on (111) $SrTiO_3$," Applied Physics Letters, **76**(20), 2937-2939 (2000). https://doi.org/10.1063/1.126522
[9] H. Jin, J. Im, and A. J. Freeman, "Topological insulator phase in halide perovskite structures," Physical Review B, **86**(12), 121102 (2012). https://doi.org/10.1103/PhysRevB.86.121102
[10] Chung, B. Lee, J. He, R. P. Chang, and M. G. Kanatzidis, "All-solid-state dye-sensitized solar cells with high efficiency," Nature, **485**(7399), 486-489 (2012). https://doi.org/10.1038/nature11067
[11] M.M. Lee, J. Teuscher, T. Miyasaka, T.N. Murakami, and H.J. Snaith, "Efficient hybrid solar cells based on meso-superstructured organometal halide perovskites," Science, **338**(6107), 643-647 (2012). https://doi.org/10.1126/science.1228604
[12] J. Burschka, N. Pellet, S.-J. Moon, R. Humphry-Baker, P. Gao, M.K. Nazeeruddin, and M. Grätzel, "Sequential deposition as a route to high-performance perovskite-sensitized solar cells," Nature, **499**(7458), 316-319 (2013). https://doi.org/10.1038/nature12340
[13] S. Kashyap, R. Pandey, J. Madan, and M.K.A. Mohammed, "Reliability Test of 21% Efficient Flexible Perovskite Solar Cell Under Concave, Convex and Sinusoidal Bending," in: *IEEE Transactions on Device and Materials Reliability*, **23**(3), 380-385 (2023). https://doi.org/10.1109/TDMR.2023.3282641
[14] S. Kashyap, *et al*., "Simulated bending test analysis of 23% efficient lead-free flexible perovskite solar cell with different bending states," Phys. Scr. 98, 114001 (2023). https://doi.org/10.1088/1402-4896/acff28
[15] Y. Takahashi, R. Obara, Z.-Z. Lin, Y. Takahashi, T. Naito, T. Inabe, S. Ishibashi, and K. Terakura, "Charge-transport in tin-iodide perovskite CH3NH3SnI3: origin of high conductivity," Dalton Transactions, **40**(20), 5563-5568 (2011). https://doi.org/10.1039/C0DT01601B

[16] X. Zhu, B. Lv, X. Shang, J. Wang, M. Li, and X. Yu, "The immobilization effects on Pb, Cd and Cu by the inoculation of organic phosphorus-degrading bacteria (OPDB) with rapeseed dregs in acidic soil," Geoderma, **350**, 1-10 (2019). https://doi.org/10.1016/j.geoderma.2019.04.015
[17] F. Geisz, M.A. Steiner, N. Jain, K.L. Schulte, R.M. France, W.E. McMahon, E.E. Perl, *et al*., "Building a six-junction inverted metamorphic concentrator solar cell," IEEE Journal of Photovoltaics, **8**(2), 626-632 (2017). https://doi.org/10.1109/JPHOTOV.2017.2778567
[18] J. Haruyama, K. Sodeyama, L. Han, and Y. Tateyama, "First-principles study of ion diffusion in perovskite solar cell sensitizers," Journal of the American Chemical Society, **137**(32), 10048-10051 (2015). https://doi.org/10.1021/jacs.5b03615
[19] Z. Li, Q. Xu, Q. Sun, Z. Hou, and W.J. Yin, "Thermodynamic stability landscape of halide double perovskites via high-throughput computing and machine learning," Advanced Functional Materials, **29**(9), 1807280 (2019). https://doi.org/10.1002/adfm.201807280
[20] Y. Zhang, *et al*., "Intrinsic instability of the hybrid halide perovskite semiconductor $CH_3NH_3PbI_3$," Chinese Physics Letters, **35**(3), 036104 (2018). https://doi.org/10.1088/0256-307X/35/3/036104
[21] Wu, J.-j. Shi, M. Zhang, Y.-l. Cen, W.-h. Guo, and Y.-h. Zhu, "Promising photovoltaic and solid-state-lighting materials: two-dimensional Ruddlesden–Popper type lead-free halide double perovskites Csn+1Inn/2Sbn/2I3n+1 (n=3) and Csn+1Inn/2Sbn/2Cl3n+1/Csm+1Cum/2Bm/2Cl3m+1(n=3, m=1)," Journal of Materials Chemistry C, **6**(43), 11575-11586 (2018). https://doi.org/10.1039/c8tc03926g
[22] J. Jiang, C.K. Onwudinanti, R.A. Hatton, P.A. Bobbert, and S. Tao, "Stabilizing lead-free all-inorganic tin halide perovskites by ion exchange," The Journal of Physical Chemistry C, **122**(31), 17660-17667 (2018). https://doi.org/10.1021/acs.jpcc.8b04013
[23] Z. Shi, *et al*., "Symmetrization of the crystal lattice of MAPbI3 boosts the performance and stability of metal–perovskite photodiodes," Advanced Materials, **29**(30), 1701656 (2017). https://doi.org/10.1002/adma.201701656
[24] M.-G. Ju, *et al*., "Toward eco-friendly and stable perovskite materials for photovoltaics," Joule, **2**(7), 1231-1241 (2018). https://doi.org/10.1016/j.joule.2018.04.026
[25] C.C. Stoumpos, *et al*., "Ruddlesden–Popper hybrid lead iodide perovskite 2D homologous semiconductors," Chemistry of Materials, **28**(8), 2852-2867 (2016). https://doi.org/10.1021/acs.chemmater.6b00847
[26] H. Chen, S. Xiang, W. Li, H. Liu, L. Zhu, and S. Yang, "Inorganic perovskite solar cells: a rapidly growing field," Solar Rrl, **2**(2), 1700188 (2018). https://doi.org/10.1002/solr.201700188
[27] Z. Deng, F. Wei, S. Sun, G. Kieslich, A. K. Cheetham, and P. D. Bristowe, "Exploring the properties of lead-free hybrid double perovskites using a combined computational-experimental approach," Journal of Materials Chemistry A, 4(31), 12025-12029 (2016). https://doi.org/10.1039/C6TA05817E
[28] W. Zhou, *et al*., "Lead-free small-bandgap $Cs_2CuSbCl_6$ double perovskite nanocrystals," The Journal of Physical Chemistry Letters, **11**(15), 6463-6467 (2020). https://doi.org/10.1021/acs.jpclett.0c01968
[29] G. Yu, *et al*., "How the Copper Dopant Alters the Geometric and Photoelectronic Properties of the Lead-Free $Cs_2AgSbCl_6$ Double Perovskite," Advanced Theory and Simulations, **4**(8), 2100142 (2021). https://doi.org/10.1002/adts.202100142
[30] M.Z. Asghar, M.A. Khan, S. Niaz, N. Noor, and A. Dahshan, "Tuning of the bandgap of Rb2ScAgX6 (X= Cl, Br, I) double perovskites through halide ion replacement for solar cell applications," Materials Science in Semiconductor Processing, **148**, 106819 (2022). https://doi.org/10.1016/j.mssp.2022.106819
[31] A. Ayyaz, G. Murtaza, A. Usman, M. Umer, M.Q. Shah, and H.S. Ali, "First principles insight on mechanical stability, optical and thermoelectric response of novel lead-free $Rb_2ScCuBr_6$ and $Cs_2ScCuBr_6$ double perovskites," Materials Science in Semiconductor Processing, **169**, 107910 (2024). https://doi.org/10.1016/j.mssp.2023.107910
[32] QuantumATK version U-2023.09, Synopsys QuantumATK (https://www.synopsys.com/silicon/quantumatk.html).
[33] J.P. Perdew, *et al*., "Atoms, molecules, solids, and surfaces: Applications of the generalized gradient approximation for exchange and correlation," Physical review B, **46**(11), 6671 (1992). https://doi.org/10.1103/PhysRevB.46.6671
[34] J.P. Perdew, K. Burke, and M. Ernzerhof, "Generalized gradient approximation made simple," Physical review letters, **77**(18), 3865 (1996). https://doi.org/10.1103/physrevlett.77.3865
[35] J. van Setten, *et al*., "The PseudoDojo: Training and grading a 85 element optimized norm-conserving pseudopotential table," Computer Physics Communications, **226**, 39-54 (2018). https://doi.org/10.1016/j.cpc.2018.01.012
[36] Q. Mahmood, *et al*., "Tunning of band gap of double perovskites halides Rb2CuSbX6 (X= Cl, Br, I) for solar cells and energy harvesting," Materials Science and Engineering: B, **286**, 116088 (2022). https://doi.org/10.1016/j.mseb.2022.116088
[37] T.-Y. Tang, and Y.-L. Tang, "Physical and optoelectronic properties of double halide perovskites $A_2CuSbX_6$ (A=Cs, Rb, K; X=Cl, Br, I) based on first principles calculations," Chemical Physics, **570**, 111897 (2023). https://doi.org/10.1016/j.chemphys.2023.111897
[38] M. Born, and K. Huang, *Dynamical theory of crystal lattices*, (Oxford university press, 1996).
[39] K. Bougherara, S. Al-Qaisi, A. Laref, T.V. Vu, and D. Rai, "Ab initio Insight of the Electronic, Structural, Mechanical and Optical Properties of X3P2 (X= Mg, Ca) from GGA and Hybrid Functional (HSE06)," Journal of Superconductivity and Novel Magnetism, **35**(1), 79-86 (2022). https://doi.org/10.1007/s10948-021-06009-3
[40] K.K. Mishra, "Study on structural, mechanical, electronic, vibrational, optical and thermo-dynamical behaviour of ZB Structured BeZ (Z= S, Se and Te) using ATK-DFT," Metallurgical and Materials Engineering, **26**(3), 253-278 (2020). https://doi.org/10.1016/j.physleta.2024.129817
[41] S. Chahar, K.K. Mishra, and R. Sharma, "Analysing the suitability of CaTiO3/Ca1–xSrxTiO3/SrTiO3 perovskite for fabrication of optoelectronic devices using QuantumATK tool: a study for electronic and optical properties," Physica Scripta, **99**(3), 035963 (2024). https://doi.org/10.1088/1402-4896/ad29cd
[42] K.K. Mishra, S. Chahar, and R. Sharma, "An extensive investigation of structural, electronic, and optical properties of inorganic perovskite $Ca_3AsCl_3$ for photovoltaic and optoelectronic applications: A first-principles approach using Quantum ATK Tool," Solid State Communications, **390**, 115623 (2024). https://doi.org/10.1016/j.ssc.2024.115623
[43] S. Chahar, K.K. Mishra, and R. Sharma, "Investigation of Structural, Electronic, and Optical Characteristics of a Novel Perovskite Halide, $Mg_3AsCl_3$, for Electronic Applications," Physica status solidi (b), 2400171 (2024). https://doi.org/10.1002/pssb.202400171

[44] S. Chahar, C. Malan, K.K. Mishra, and R. Sharma, "Optimizing novel perovskite $Mg_3AsBr_3$ through uniaxial stress: A comprehensive study of its potential in solar and optoelectronic applications," Physica Scripta, **99**, 095994 (2024): https://doi.org/10.1088/1402-4896/ad6bd1
[45] D. Schwartz, et al., "Air Stable, High-Efficiency, Pt-Based Halide Perovskite Solar Cells with Long Carrier Lifetimes," Physica status solidi (RRL)–Rapid Research Letters, **14**(8), 2000182 (2020). https://doi.org/10.1002/pssr.202000182
[46] L.K. Gautam, H. Haneef, M. Junda, D.S. John, and N. Podraza, "Approach for extracting complex dielectric function spectra in weakly-absorbing regions," Thin Solid Films, **571**, 548-553 (2014). https://doi.org/10.1016/j.tsf.2014.03.020

## ПОТЕНЦІАЛ ПОДВІЙНИХ ГАЛОГЕНІДІВ ПЕРОВСКІТУ $Rb_2CuSbH_6$ (H = Cl, Br, I) ДЛЯ ГНУЧКОЇ ЕЛЕКТРОНІКИ: КОМПЛЕКСНЕ ДОСЛІДЖЕННЯ СТРУКТУРНИХ, МЕХАНІЧНИХ, ЕЛЕКТРИЧНИХ ТА ОПТИЧНИХ ВЛАСТИВОСТЕЙ

**Крішна Кумар Мішра[a], Соня Чахар[a], Раджніш Шарма[b]**
*[a]Інститут інженерії та технології Університету Чіткара, Університет Чіткара, Раджпура, Пенджаб-140401, Індія*
*[b]Школа інженерії та технології, Університет Чіткара, Солан, Гімачал-Прадеш-174103, Індія*

Структурні, механічні, електричні та оптичні властивості подвійних галогенідів перовскіту, таких як $Rb_2CuSbH_6$ (де H = Cl, Br та I) для гнучких електронних пристроїв, захоплюючі та складні. Дослідження літератури чітко встановлює, що дослідження щодо аналізу потенційного використання цих матеріалів у дуже затребуваному секторі гнучких електронних пристроїв були обмежені. У цій статті були проведені цілеспрямовані дослідження щодо вивчення характеристик цих матеріалів за допомогою програмного засобу QuantumATK NanoLab. Усі галогеніди подвійного перовскіту $Rb_2CuSbH_6$ (H = Cl, Br, I) демонструють позитивні значення пружних констант C11, C12 та C44 і підкоряються тенденції стабільності C11>C12>C44. Механічну стабільність встановлювали за критеріями Борна-Хуанга. Оптимізовані значення модуля Юнга, модуля об'ємної пружності, модуля зсуву та коефіцієнтів Пуассона встановили, що матеріали є стабільними та пластичними за своєю природою. Під час проведення аналізу електронних властивостей було виявлено, що всі три матеріали $Rb_2CuSbCl_6$, $Rb_2CuSbBr_6$ і Rb2CuSbI$_6$ мають непряму заборонену зону 0,924 еВ, 0,560 еВ і 0,157 еВ відповідно. Більше того, природність комплексної смугової структури (CB) вказує на те, що найбільша кількість хвиль, що завмирають, може існувати, коли поділ шарів найменший у $Rb_2CuSbCl_6$ (6,0 Å), $Rb_2CuSbBr_6$ (6,33 Å) і найвищий у $Rb_2CuSbI_6$ (6,8 Å). Смуги поглинання для Rb2CuSbCl6, Rb2CuSbBr6 і Rb2CuSbI6 лежать у видимому діапазоні від 344 нм до 574 нм, від 348 нм до 688 нм і від 369 нм до 608 нм відповідно. Коефіцієнт відбиття (r), зазначений у цьому дослідженні, становить 0,105, 0,139 і 0,185 відповідно для $Rb_2CuSbCl_6$, $Rb_2CuSbBr_6$ і $Rb_2CuSbI_6$. Загалом, усі отримані результати вказують на необхідність більш глибокого вивчення матеріалів $Rb_2CuSbH_6$ для різних застосувань електронних пристроїв.

Ключові слова: *перовскіт; QuantumATK; DFT; оптичні властивості; електронна структура; механічні властивості*